Wave Drift Forces' Calculation on Two Floating Bodies Based on the Boundary Element Method—Attempt for Improvement of the Constant Panel Method

Qiao Li
Institute of Industrial Science,
The University of Tokyo,
Kashiwa 2778574, Japan;
Graduate School of Engineering,
Osaka Prefecture University,
Osaka 5998531, Japan
e-mail: liqiao23@hotmail.com

Yasunori Nihei
Graduate School of Engineering,
Osaka Prefecture University,
Osaka 5998531, Japan
e-mail: nihei@marine.osakafu-u.ac.jp

An improved constant panel method for more accurate evaluation of wave drift forces and moment is proposed. The boundary element method (BEM) of solving boundary integral equations is used to calculate velocity potentials of floating bodies. The equations are discretized by either the higher-order boundary element method or the constant panel method. Though calculating the velocity potential via the constant panel method is simple, the results are unable to accurately evaluate wave drift forces and moment. An improved constant panel method is introduced to address these issues. The improved constant panel method can, without difficulty, employ the near-field method to evaluate wave drift forces and moment, especially for multiple floating bodies. Results of the new evaluation method will be compared with other evaluation method. Additionally, hydrodynamic interaction between multiple floating bodies will be assessed.
[DOI: 10.1115/1.4042180]

1 Introduction

Floating production storage and offloading systems including floating liquefied natural gas vessels exemplify a system of two floating bodies. Such a system necessitates a numerical calculation method to predict the fluid forces concerning the bodies' hydrodynamic interactions. The far-field method and near-field method are available for evaluating wave drift forces and moment. Newman [1] and Maruo [2] proposed the far-field method, which is based on the momentum conservation principle. This method is always used for single floating body because it considers all forces and moment acting on all bodies within the domain of a fictitious vertical cylinder far from the bodies. Kashiwagi et al. [3] developed the far-field method for multiple floating bodies if the vertical cylinders surrounding the floating bodies do not overlap. Alternatively, the near-field method integrates pressure across the wetted surface of each floating body [4–6], and can be used to evaluate wave drift forces, moment, as well as local pressure on each floating body. In either method, accurate evaluation of velocity potentials of the floating bodies is crucial.

The velocity potential of the floating bodies is found by using the boundary element method (BEM) to solve the boundary integral equations derived from Green's function and the linearized boundary conditions [7]. Two methods are available to discretize the boundary integral equations, the constant panel method and HOBEM. Though the constant panel method [8] is itself simple to employ, the resulting velocity potentials are inaccurate compared to the HOBEM. Additionally, the resulting velocity potentials cannot accurately evaluate wave drift forces and moment by near-field method, because the velocity potentials are not representative of the water line. Finally, it is difficult to evaluate differential value of velocity potentials with high precision. Söding [9] introduced a new numerical method, which uses Rankine sources to accurately predict pressure and forces on a constant panel. Furthermore, Söding et al. [10] presented a method of calculating ship drift forces in waves using constant panels. To ascertain high computational precision of velocity panels, many studies utilize HOBEM with seven and nine-point isoparametric representations of the velocity potentials for comparative analysis (e.g., see Refs. [3] and [11]).

This paper proposes a numerical technique to solve the aforementioned issues concerning inaccuracy at the water line and the difficulties regarding velocity potential differential calculations. Through this new technique, the near-field method can be used with ease to calculate wave drift forces and moment. Two modules will be introduced by this technique, the extrapolation function, and isoparametric elements. The velocity potential obtained from the constant panel method on the floating bodies is extrapolated to the other points, including the water line, to resolve the former issue. These more representative velocity potentials are used by the near-field method to calculate wave drift forces and moment. The formulation of isoparametric elements serves to simplify the differential calculations. To test the accuracy of the proposed technique, the fluid forces of an ellipsoidal floating body are calculated by the new numerical method and compared with the conventional constant panel method and HOBEM. Additionally, the new numerical method is applied to two floating bodies arranged in tandem to assess various drift forces and moments, and the effects of distance on hydrodynamic interactions between floating bodies.

2 Boundary Element Method and Conventional Solution Method

2.1 Boundary Value Problem. As shown in Fig. 1, the global coordinate system *xyz* is used throughout this paper, with the *xy*-plane representing the undisturbed water surface, and *z* extending positively into the sea floor. In addition to the global coordinate system, two local coordinate systems are introduced:

Paper presented at the 2016 ASME 35th International Conference on Ocean, Offshore, and Arctic Engineering (OMAE2016), Busan, Korea, June 19-24, 2016,Paper No. OMAE2016-54263.

Contributed by the Ocean, Offshore, and Arctic Engineering Division of ASME for publication in the Journal of Offshore Mechanics and Arctic Engineering. Manuscript received July 11, 2017; final manuscript received November 30, 2018; published online January 17, 2019. Assoc. Editor: Ould el Moctar.

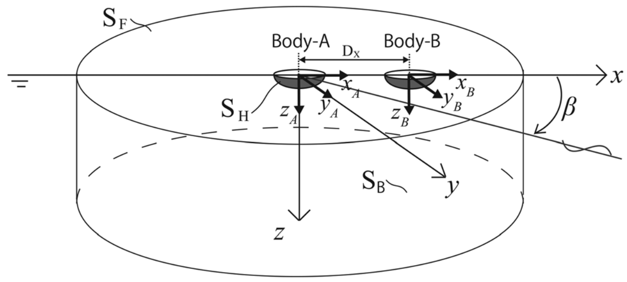

Fig. 1 Calculating domain

$x_Ay_Az_A$ in body-A and $x_By_Bz_B$ in body-B. S_H is the wetted body surface, S_F is the free surface, and S_B is the water bottom.

The floating bodies are assumed to oscillate in time as a sinusoid with circular frequency ω. The velocity potential of the first-order incident wave is expressed as

$$\Phi(x, y, z, t) = \mathrm{Re}[\phi(x, y, z)e^{i\omega t}] \tag{1}$$

The velocity potential, which satisfies the above governing equation and linearized boundary conditions, is summarized as follows:

$$[\mathrm{L}] \quad \frac{\partial^2\phi}{\partial x^2} + \frac{\partial^2\phi}{\partial y^2} + \frac{\partial^2\phi}{\partial z^2} = 0 \quad \text{for } z \geq 0 \tag{2}$$

$$[\mathrm{F}] \quad \frac{\partial\phi}{\partial z} + K\phi = 0 \quad \text{on } S_F\ (z = 0) \tag{3}$$

$$[\mathrm{B}] \quad \frac{\partial\phi}{\partial z} = 0 \qquad \text{as } z \to \infty \tag{4}$$

$$[\mathrm{H}] \quad \frac{\partial\phi}{\partial n} = 0 \quad \text{on } S_H \tag{5}$$

Equation (2) is the Laplace equation in the fluid domain; Eq. (3) is the linear free surface condition ($K = \omega^2/g$); Eq. (4) is a condition on the sea bottom; and Eq. (5) is the conditions across the wetted surface of the body surface.

2.2 Boundary Integral Equation and Discretization of the Constant Panel Method. The free-surface Green's function $G(P, Q)$ is used to solve the first-order boundary value problem. The constant panel method is used to solve the diffraction integral equation for the velocity potentials given by

$$\frac{1}{2}\phi_D(P) + \iint_{S_H} \phi_D(Q)\frac{\partial G(P;Q)}{\partial n_Q}dS(Q) = \phi_0(P) \tag{6}$$

where $P = (x, y, z)$ is the point on the field and $Q = (x', y', z')$ is the source on the floating body. The constant panel method is used to solve for the diffraction velocity potential $\phi_D(P)$ in Eq. (6).

The Green's function of the unbound fluid in three dimensions is given by

$$\begin{cases} G(P,Q) = -\dfrac{1}{4\pi r} \\ r = \sqrt{(x-x')^2 + (y-y')^2 + (z-z')^2} \end{cases} \tag{7}$$

and assuming N panels on the surface of the floating body, the potential ϕ is

$$2\pi\phi_D(P_m) = \sum_{n=1}^{N}\phi_D(Q_n)\mathcal{D}_{mn} - \sum_{n=1}^{N}\left(\frac{\partial\phi_D(Q_n)}{\partial n}\right)\mathcal{S}_{mn}\ (m = 1, \ldots, N; n = 1, \ldots, N) \tag{8}$$

where

$$\begin{aligned} \mathcal{D}_{mn} &= \iint_{S_{Hn}} \frac{\partial}{\partial n}\left(\frac{1}{r}\right)ds(Q) \\ \mathcal{S}_{mn} &= \iint_{S_{Hn}} \frac{1}{r}ds(Q) \quad r = r(P_m, Q) \end{aligned} \tag{9}$$

$\mathcal{D}_{mn}$ and $\mathcal{S}_{mn}$ may be computed using the local coordinate system for each panel to be calculated [12]. $\mathcal{D}_{mn}$ and $\mathcal{S}_{mn}$ can be discretized as

$$\begin{aligned} \mathcal{D} &= \iint\left[\frac{\partial}{\partial z'}\left(\frac{1}{r}\right)\right]_{z'=0}dx'dy' = \sum_{n=1}^{4}\tan^{-1}\left(\frac{B_1A_2 - B_2A_1}{A_1A_2 + B_1B_2}\right) \\ \mathcal{S} &= \iint\frac{1}{r}dx'dy' \\ &= \sum_{n=1}^{4}\left[(x-x'_n)\frac{\partial y'_n}{s_n} - (y-y'_n)\frac{\partial x'_n}{s_n}\right] \times \log\left(\frac{R_n + R_{n+1} + s_n}{R_n + R_{n+1} - s_n}\right) - z\mathcal{D} \end{aligned} \tag{10}$$

where

$$\begin{cases} A_1 = R_n z\delta x'_n \\ B_1 = \delta y'_n[(x-x'_n)^2 + z^2] - \delta x'_n(x-x'_n)(y-y'_n) \\ A_2 = R_{n+1}z\delta x'_n \\ B_2 = \delta y'_n[(x-x\prime_{n+1})^2 + z^2] - \delta x'_n(x-x'_{n+1})(y-y'_{n+1}) \end{cases} \tag{11}$$

and

$$\begin{cases} \delta x'_n = x'_{n+1} - x'_n \\ \delta y'_n = y'_{n+1} - y'_n \\ R_n = \sqrt{(x-x'_n)^2 + (y-y'_n)^2 + z^2} \\ R_{n+1} = \sqrt{(x-x'_{n+1})^2 + (y-y'_{n+1})^2 + z^2} \end{cases} \tag{12}$$

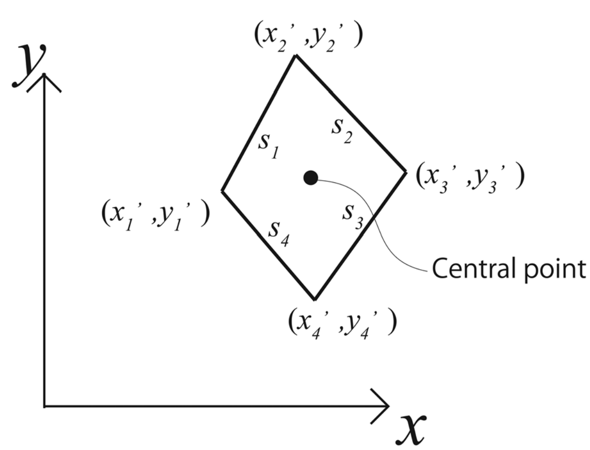

Fig. 2 Local coordinate system

For Fig. 2, in the local coordinate system $x = x'_n$ and $y = y'_n$, s_n denotes the panel side's length, and n denotes panel side, $n = 1 \ldots 4$. For each panel, the calculated diffraction velocity potential $\phi_D(P)$ is measured at the center of the panel.

2.3 Boundary Integral Equation for Two Floating Bodies. To compute the velocity potential of two bodies, their hydrodynamic interaction must be considered. As shown in Fig. 1, the surfaces of bodies A and B can be discretized into panels $S_{n_A}(n_A = 1 \sim N_A)$ and $S_{n_B}(n_B = 1 \sim N_B)$, respectively. The total number of panels $N_{\text{all}} = N_A + N_B$. To evaluate the diffraction velocity potential of two bodies, Eq. (6) is rewritten as

$$\frac{1}{2}\phi_D(P_m) + \sum_{n=1}^{N_{\text{all}}} \phi_D(Q_n) \frac{\partial}{\partial n_Q} G(P_m; Q_n) dS = \phi_0(P_m) \tag{13}$$

The resulting $N_{\text{all}} \times N_{\text{all}}$ equations can be solved similar to the case of the single floating body. The equations can be represented by $[T_{mn}]$ as

$$[T_{mn}] = \left(\begin{array}{ccc|ccc} N_{1,1} & \cdots & N_{1,N_A} & N_{1,N_A+1} & \cdots & N_{1,N_A+N_B} \\ \vdots & \ddots \underline{I} & \vdots & \vdots & \ddots \underline{II} & \vdots \\ N_{N_A,1} & \cdots & N_{N_A,N_A} & N_{N_A,1} & \cdots & N_{N_A,N_A+N_B} \\ \hline N_{N_A+1,1} & \cdots & N_{N_A+1,N_A} & N_{N_A+1,1} & \cdots & N_{N_A+1,N_A+N_B} \\ \vdots & \ddots \underline{III} & \vdots & \vdots & \ddots \underline{IV} & \vdots \\ N_{N_A+N_B,1} & \cdots & N_{N_A+N_B,N_A} & N_{N_A+N_B,1} & \cdots & N_{N_A+N_B,N_A+N_B} \end{array}\right) \tag{14}$$

Section *I* represents the single body equations for body-A. Section *II* represents the hydrodynamic effects of body-B on body-A. Section *III* represents the hydrodynamic effects of body-A on body-B. Section *IV* represents the single body equations for body-B. Therefore, the totality of hydrodynamic interactions of the two bodies is considered in the numerical solutions.

2.4 Calculation of Wave Drift Forces by the Near-Field Method. The wave drift forces and moment can be obtained by taking a time average over one period of the second-order forces, which can be computed by integrating the pressure on the surface of the floating body as follows

$$F_q = -\iint_{S_H} p n_q dS \tag{15}$$

in the x- and y-direction ($q = 1$ and 2). Using Bernoulli's principle

$$p = \rho\left[-\frac{\partial \Phi}{\partial t} - \frac{1}{2}\{|\nabla\Phi|^2\} - gZ\right] \tag{16}$$

The second-order forces can be computed as follows

$$F_q = \frac{\rho}{2}\iint_{S_H} |\nabla\Phi|^2 n_q dS - \frac{1}{2}\rho g \oint_{Cw} \zeta^2 \times n_q dl \tag{17}$$

where C_w denotes the water line and ζ is calculated as follows

$$\zeta = -\frac{1}{g}\frac{\partial\Phi}{\partial t}\bigg|_{z=0} \tag{18}$$

Similarly, the second-order moment can be obtained as follows

$$M_z = \frac{\rho}{4}\iint_{S_H} |\nabla\Phi|^2 (zn_y - yn_x) dS - \rho g \oint_{Cw} \zeta^2 \times (xn_y - yn_x) dl \tag{19}$$

Referring to an established second-order theory using the consistent perturbation scheme (e.g., see Refs. [10] and [13]), the time average of the time-dependent exponential, $e^{i\omega t}$ in Eq. (1), can be evaluated according to the following formula:

$$\overline{\text{Re}[Ae^{i\omega t}]\,\text{Re}[Be^{i\omega t}]} = \frac{1}{2}\text{Re}[AB^*] \tag{20}$$

where * denotes the complex conjugate.

As a result, when the floating bodies are restrained in motion, the equations for the time-averaged steady forces and moments include only the diffraction components. The nondimensional equations for drift forces $\overline{F_q}$ and moment $\overline{M_Z}$ are as follows:

$$\frac{\overline{F_q}}{\frac{1}{2}\rho g \zeta_w^2 L} = \frac{1}{2}\left[\frac{1}{K}\iint_{S_H} |\nabla\phi_D|^2 n_q dS - \oint_{Cw} |\nabla\phi_D|^2 n_q dl\right] \tag{21}$$

$$\frac{\overline{M_z}}{\frac{1}{2}\rho g \zeta_w^2 L^2} = \frac{1}{2}\left[\frac{1}{K}\iint_{S_H} |\nabla\phi_D|^2 (zn_y - yn_x) dS - \oint_{Cw} |\nabla\phi_D|^2 (xn_y - yn_x) dl\right] \tag{22}$$

where the overbar denotes the time average, ζ_w denotes the wave height, and the L denotes the length of floating body.

3 Formulation of New Numerical Technique

Evaluating the wave drift forces and moment using the near-field method is inaccurate because the velocity potential derived from the constant panel method only yields velocity potentials representative of the center of the panel, thus making the contour integral along the water line C_w, in Eqs. (21) and (22), difficult. Additionally, evaluating the velocity potential differential (the double integral in Eqs. (21) and (22)) is also difficult.

To resolve the velocity potential inaccuracies along the water line, the extrapolation function is introduced. The new constant panel method uses the conventional constant panel method to obtain the velocity potential of the floating body, and extrapolates the velocity potential of other points on the panels, some of which are representative of the water line, thus providing accurate velocity potentials along the water line C_w. The resulting velocity potential extrapolations are used for the generation of isoparametric elements. These isoparametric elements are used to solve the velocity potential differential.

3.1 Formulation of the Extrapolation Function. When computing the velocity potential on the water line C_w (second

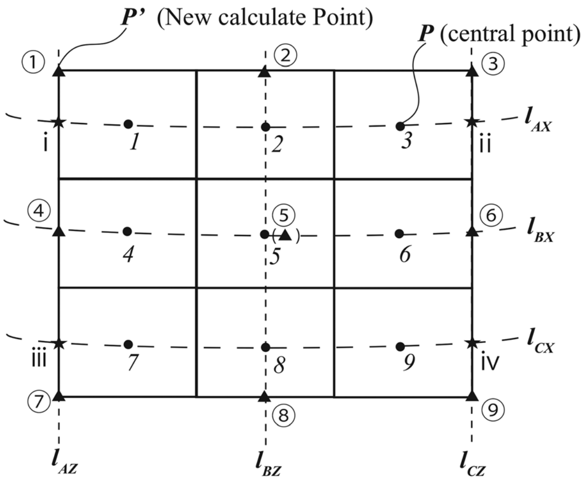

Fig. 3 Evaluation points used in the conventional and the new constant panel method

terms on the right-hand sides of Eqs. (21) and (22)), the quadratic extrapolation function can be used to calculate the velocity potential ϕ and the normal vector $\mathbf{n}$ of the new evaluation points. The positional relationship between the new evaluation points and the center point of the conventional constant panel method is defined in Fig. 3. The circular points are those used in the conventional calculation (center points P), and the triangular points are the new evaluation points P'. Here, 1–9 denote the numbers of the center points, and ① ~ ⑨ denote the numbers of the new evaluation points. Moreover, i–iv are the auxiliary points that are obtained in the extrapolation. l_{AX}, l_{BX}, and l_{CX} are the trend lines in the x direction, and l_{AZ}, l_{BZ}, and l_{CZ} are the trend lines in the z direction.

Along line l_{AX} in the x-axis, the quadratic elements $a_{l_{AX}}$, $b_{l_{AX}}$, and $c_{l_{AX}}$, based on ϕ and the x coordinates of points 1, 2, and 3, are formulated as follows:

$$\begin{pmatrix} x_1^2 & x_1 & 1 \\ x_2^2 & x_2 & 1 \\ x_3^2 & x_3 & 1 \end{pmatrix} \begin{pmatrix} a_{l_{AX}} \\ b_{l_{AX}} \\ c_{l_{AX}} \end{pmatrix} = \begin{pmatrix} \phi_1 \\ \phi_2 \\ \phi_3 \end{pmatrix} \tag{23}$$

The velocity potential ϕ_i and ϕ_{ii} can be computed with the above coefficients as follows:

$$\mathrm{i}\ :\ \phi_{\mathrm{i}} = a_{l_{AX}} x_{\mathrm{i}}^2 + b_{l_{AX}} x_{\mathrm{i}} + c_{l_{AX}} \tag{24}$$

$$\mathrm{ii}\ :\ \phi_{\mathrm{ii}} = a_{l_{AX}} x_{\mathrm{ii}}^2 + b_{l_{AX}} x_{\mathrm{ii}} + c_{l_{AX}} \tag{25}$$

The velocity potentials $\phi_④, \phi_⑥, \phi_{\mathrm{iii}}$, and ϕ_{iv} can be obtained using the same method along lines l_{BX} and l_{CX}.

Along line l_{AZ} in the z axis, the quadratic elements $a_{l_{AZ}}$, $b_{l_{AZ}}$, and $c_{l_{AZ}}$ can be formulated as follows:

$$\begin{pmatrix} x_{\mathrm{i}}^2 & x_{\mathrm{i}} & 1 \\ x_④^2 & x_④ & 1 \\ x_{\mathrm{iii}}^2 & x_{\mathrm{iii}} & 1 \end{pmatrix} \begin{pmatrix} a_{l_{AZ}} \\ b_{l_{AZ}} \\ c_{l_{AZ}} \end{pmatrix} = \begin{pmatrix} \phi_{\mathrm{i}} \\ \phi_④ \\ \phi_{\mathrm{iii}} \end{pmatrix} \tag{26}$$

Similarly, velocity potentials $\phi_①$ and $\phi_⑦$ can be computed as follows:

$$①\ :\ \phi_① = a_{l_{AZ}} x_①^2 + b_{l_{AZ}} x_① + c_{l_{AZ}} \tag{27}$$

$$⑦\ :\ \phi_⑦ = a_{l_{AZ}} x_⑦^2 + b_{l_{AZ}} x_⑦ + c_{l_{AZ}} \tag{28}$$

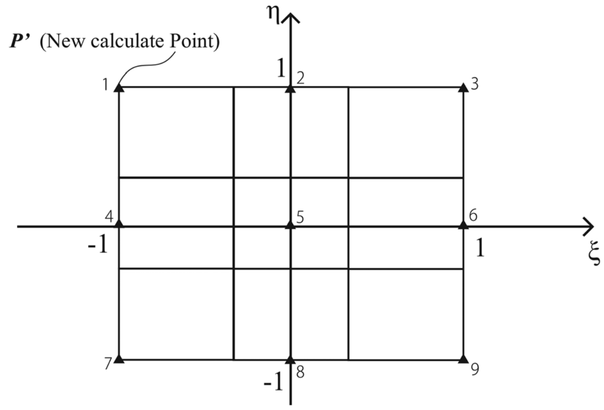

Fig. 4 Isoparametric elements

The velocity potentials $\phi_②$, $\phi_⑧$, $\phi_③$, and $\phi_⑨$ can be obtained using the same method along lines l_{BZ} and l_{CZ}.

Thus, the velocity potentials have been successfully extrapolated from ϕ_1–ϕ_9 to the new evaluation points $\phi_① - \phi_⑨$

$$\begin{cases} \phi_① = a_{l_{AZ}} x_①^2 + b_{l_{AZ}} x_① + c_{l_{AZ}} \\ \phi_② = a_{l_{BZ}} x_②^2 + b_{l_{BZ}} x_② + c_{l_{BZ}} \\ \phi_③ = a_{l_{CZ}} x_③^2 + b_{l_{CZ}} x_③ + c_{l_{CZ}} \\ \phi_④ = a_{l_{BX}} x_④^2 + b_{l_{BX}} x_④ + c_{l_{BX}} \\ \phi_⑤ = \phi_5 \\ \phi_⑥ = a_{l_{BX}} x_⑥^2 + b_{l_{BX}} x_⑥ + c_{l_{BX}} \\ \phi_⑦ = a_{l_{AZ}} x_⑦^2 + b_{l_{AZ}} x_⑦ + c_{l_{AZ}} \\ \phi_⑧ = a_{l_{BZ}} x_⑧^2 + b_{l_{BZ}} x_⑧ + c_{l_{BZ}} \\ \phi_⑨ = a_{l_{CZ}} x_⑨^2 + b_{l_{CZ}} x_⑨ + c_{l_{CZ}} \end{cases} \tag{29}$$

These new extrapolated velocity potentials along the water line can be used to solve the contour integral in Eqs. (21) and (22).

3.2 Formulation of the Isoparametric Elements. Formulating the isoparametric elements using the new extrapolated points is used to solve the double integral in Eqs. (21) and (22). Figure 4 shows the utilization of isoparametric elements. The velocity potential can be obtained as follows:

$$\begin{aligned} \phi = a_0 + a_1\xi + a_2\eta + a_3\xi\eta + a_4\xi^2 + a_5\eta^2 \\ + a_6\xi^2\eta + a_7\xi\eta^2 + a_8\xi^2\eta^2 \end{aligned} \tag{30}$$

where the ξ and η are positional coordinates of values 1, −1, or 0

$$\begin{cases} \phi_1 = a_0 - a_1 + a_2 - a_3 + a_4 + a_5 + a_6 - a_7 + a_8 \\ \phi_2 = a_0 + a_2 + a_5 \\ \phi_3 = a_0 + a_1 + a_2 + a_3 + a_4 + a_5 + a_6 + a_7 + a_8 \\ \phi_4 = a_0 - a_1 + a_4 \\ \phi_5 = a_0 \\ \phi_6 = a_0 + a_1 + a_4 \\ \phi_7 = a_0 - a_1 - a_2 + a_3 + a_4 + a_5 - a_6 - a_7 + a_8 \\ \phi_8 = a_0 - a_2 + a_5 \\ \phi_9 = a_0 + a_1 - a_2 - a_3 + a_4 + a_5 - a_6 + a_7 + a_8 \end{cases} \tag{31}$$

Through rearrangement, Eq. (30) is written as follows:

$$
\begin{aligned}
\phi = {} & \phi_5 + \frac{1}{2}(\phi_6 - \phi_4)\xi - \frac{1}{2}(\phi_5 - \phi_7)\eta \\
& + \frac{1}{4}(\phi_7 - \phi_9 + \phi_3 - \phi_4)\xi\eta \\
& + \left\{\frac{1}{2}(\phi_6 + \phi_4) - \phi_5\right\}\xi^2 + \left\{\frac{1}{2}(\phi_8 + \phi_2) - \phi_5\right\}\eta^2 \\
& + \left\{-\frac{1}{4}(\phi_7 + \phi_9 - \phi_3 - \phi_1) + \frac{1}{2}(\phi_8 - \phi_2)\right\}\xi^2\eta \\
& + \left\{-\frac{1}{4}(\phi_7 - \phi_9 - \phi_3 + \phi_1) - \frac{1}{2}(\phi_6 - \phi_4)\right\}\xi\eta^2 \\
& + \left\{\frac{1}{4}(\phi_7 + \phi_9 + \phi_3 + \phi_1) - \frac{1}{2}(\phi_8 + \phi_6 + \phi_2 + \phi_4) + \phi_5\right\}\xi^2\eta^2 \\
\equiv {} & \sum_{k=1}^{9} N_k(\xi,\eta)\phi_k
\end{aligned}
\tag{32}
$$

where N_k denotes the isoparametric elements decomposed as follows:

$$
\begin{cases}
N_1 = \frac{1}{4}\xi(\xi-1)\eta(\eta+1) \\
N_2 = \frac{1}{2}\eta(\eta+1)(1-\xi^2) \\
N_3 = \frac{1}{4}\xi(\xi+1)\eta(\eta+1) \\
N_4 = \frac{1}{2}\xi(\xi-1)(1-\eta^2) \\
N_5 = (1-\xi^2)(1-\eta^2) \\
N_6 = \frac{1}{2}\xi(\xi+1)(1-\eta^2) \\
N_7 = \frac{1}{4}\xi(\xi-1)\eta(\eta-1) \\
N_8 = \frac{1}{2}\eta(\eta-1)(1-\xi^2) \\
N_9 = \frac{1}{4}\xi(\xi+1)\eta(\eta-1)
\end{cases}
\tag{33}
$$

Their derivative with respect to ξ as follows:

$$
\begin{cases}
\frac{\partial N_1}{\partial \xi} = \frac{1}{4}(2\xi-1)\eta(\eta+1) \\
\frac{\partial N_2}{\partial \xi} = -\eta(\eta+1)\xi \\
\frac{\partial N_3}{\partial \xi} = \frac{1}{4}(2\xi+1)\eta(\eta+1) \\
\frac{\partial N_4}{\partial \xi} = \frac{1}{2}(2\xi-1)(1-\eta^2) \\
\frac{\partial N_5}{\partial \xi} = -2\xi(1-\eta^2) \\
\frac{\partial N_6}{\partial \xi} = \frac{1}{2}(2\xi+1)(1-\eta^2) \\
\frac{\partial N_7}{\partial \xi} = \frac{1}{4}(2\xi-1)\eta(\eta-1) \\
\frac{\partial N_8}{\partial \xi} = -\eta(\eta-1)\xi \\
\frac{\partial N_9}{\partial \xi} = \frac{1}{4}(2\xi+1)\eta(\eta-1)
\end{cases}
\tag{34}
$$

Similarly, their derivative with respect to η can be evaluated. $((\partial\phi/\partial x), (\partial\phi/\partial y), (\partial\phi/\partial z))$ can then be evaluated using the isoparametric elements and their derivatives as follows:

$$
\frac{\partial \phi}{\partial x} = \frac{1}{|\mathbf{a}\times\mathbf{b}|}\left\{n_Z\left(\frac{\partial\phi}{\partial\xi}\frac{\partial y}{\partial\eta} - \frac{\partial\phi}{\partial\eta}\frac{\partial y}{\partial\xi}\right) - n_Y\left(\frac{\partial\phi}{\partial\xi}\frac{\partial Z}{\partial\eta} - \frac{\partial\phi}{\partial\eta}\frac{\partial z}{\partial\xi}\right)\right\}
\tag{35}
$$

$$
\frac{\partial \phi}{\partial y} = \frac{1}{|\mathbf{a}\times\mathbf{b}|}\left\{n_X\left(\frac{\partial\phi}{\partial\xi}\frac{\partial z}{\partial\eta} - \frac{\partial\phi}{\partial\eta}\frac{\partial z}{\partial\xi}\right) - n_Z\left(\frac{\partial\phi}{\partial\xi}\frac{\partial X}{\partial\eta} - \frac{\partial\phi}{\partial\eta}\frac{\partial x}{\partial\xi}\right)\right\}
\tag{36}
$$

$$
\frac{\partial \phi}{\partial z} = \frac{1}{|\mathbf{a}\times\mathbf{b}|}\left\{n_Y\left(\frac{\partial\phi}{\partial\xi}\frac{\partial x}{\partial\eta} - \frac{\partial\phi}{\partial\eta}\frac{\partial x}{\partial\xi}\right) - n_X\left(\frac{\partial\phi}{\partial\xi}\frac{\partial Y}{\partial\eta} - \frac{\partial\phi}{\partial\eta}\frac{\partial y}{\partial\xi}\right)\right\}
\tag{37}
$$

where

$$
\mathbf{a} = \left(\frac{\partial x}{\partial\xi}, \frac{\partial y}{\partial\xi}, \frac{\partial z}{\partial\xi}\right), \quad \mathbf{b} = \left(\frac{\partial x}{\partial\eta}, \frac{\partial y}{\partial\eta}, \frac{\partial z}{\partial\eta}\right)
\tag{38}
$$

Their derivatives with respect to ξ and η can be computed from the isoparametric elements as follows:

$$
\{\phi, x, y, z\} = \sum_{k=1}^{9} N_k(\xi,\eta)\{\phi_k, x_k, y_k, z_k\}
\tag{39}
$$

$$
\left\{\frac{\partial\phi}{\partial\xi}, \frac{\partial x}{\partial\xi}, \frac{\partial y}{\partial\xi}, \frac{\partial z}{\partial\xi}\right\} = \sum_{k=1}^{9}\frac{\partial N_k}{\partial\xi}\{\phi_k, x_k, y_k, z_k\}
\tag{40}
$$

$$
\left\{\frac{\partial\phi}{\partial\eta}, \frac{\partial x}{\partial\eta}, \frac{\partial y}{\partial\eta}, \frac{\partial z}{\partial\eta}\right\} = \sum_{k=1}^{9}\frac{\partial N_k}{\partial\eta}\{\phi_k, x_k, y_k, z_k\}
\tag{41}
$$

Thus, with the new constant panel method, accurate velocity potential differential calculations can be obtained.

4 Results and Discussion

4.1 Calculation of Single Floating Body. For comparative analysis, the results of a floating body of ellipsoid geometry are analyzed. The ellipsoid parameterizations are as follows:

$$
\begin{aligned}
x &= a\cos\varphi \\
y &= b\sin\varphi\cos\vartheta \\
z &= c\sin\varphi\sin\vartheta (z \geq 0)
\end{aligned}
\tag{42}
$$

where a, b, and c denote the half-length, the half-breadth, and the draft of the ellipsoid. The parametric variables φ and ϑ vary from 0 to π. The shape of the ellipsoid is shown in Fig. 5. The length

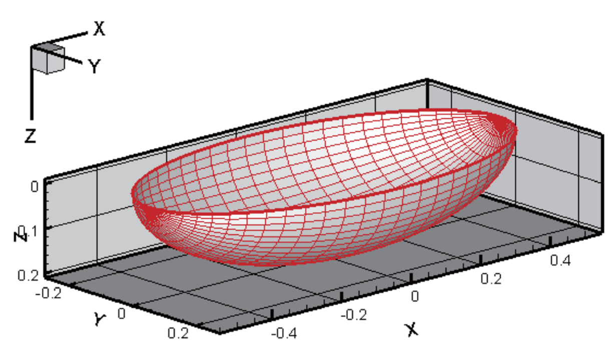

Fig. 5 Calculation model of an ellipsoid body

Table 1 Convergence of the results with different mesh numbers

N_E	$\lambda/L=0.3$	0.5	1.0
6×6	357.70%	−50.02%	−0.50%
12×12	10.55%	−1.98%	0.00%
18×18	2.62%	−0.78%	0.01%
24×24	1.22%	−0.27%	0.01%
30×30	0.62%	−0.19%	0.01%
36×36	0.30%	−0.09%	0.00%
42×42	0.12%	−0.04%	0.00%
48×48	0.00%	0.00%	0.00%

(L), breadth (B), and draft (D) of the ellipsoid are 1.0, 0.5, and 0.2, respectively. The number of discretized elements on the surface of the ellipsoid is $30\times 30=900$.

4.1.1 Decision of the Number of Elements. To ensure computational speed and accuracy, both the numerical method and the number of elements must be considered. Generally, the greater the number of elements, the greater the computational accuracy. However, this also increases the computational load and thus the computation time. Fortunately, as the number of elements and computational accuracy increase, it reaches a point where an additional number of elements does not change the result, hinting at a convergence of results. Therefore, setting an appropriate number of elements is a crucial step in performing high precision calculations at an appropriate speed.

To extract the appropriate of elements, the number of elements N_E varies from 6×6 to 48×48 in increments 6×6, while the results are stored for analysis

$$A=\iint_{S_H}\phi_D dS \tag{43}$$

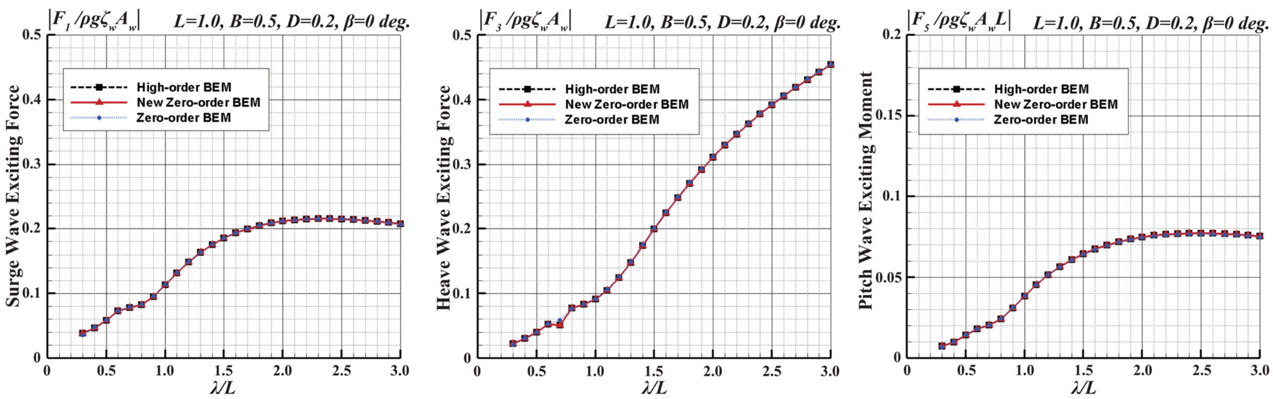

Fig. 6 Wave exciting forces and moments of single body ($\beta=0$ deg)

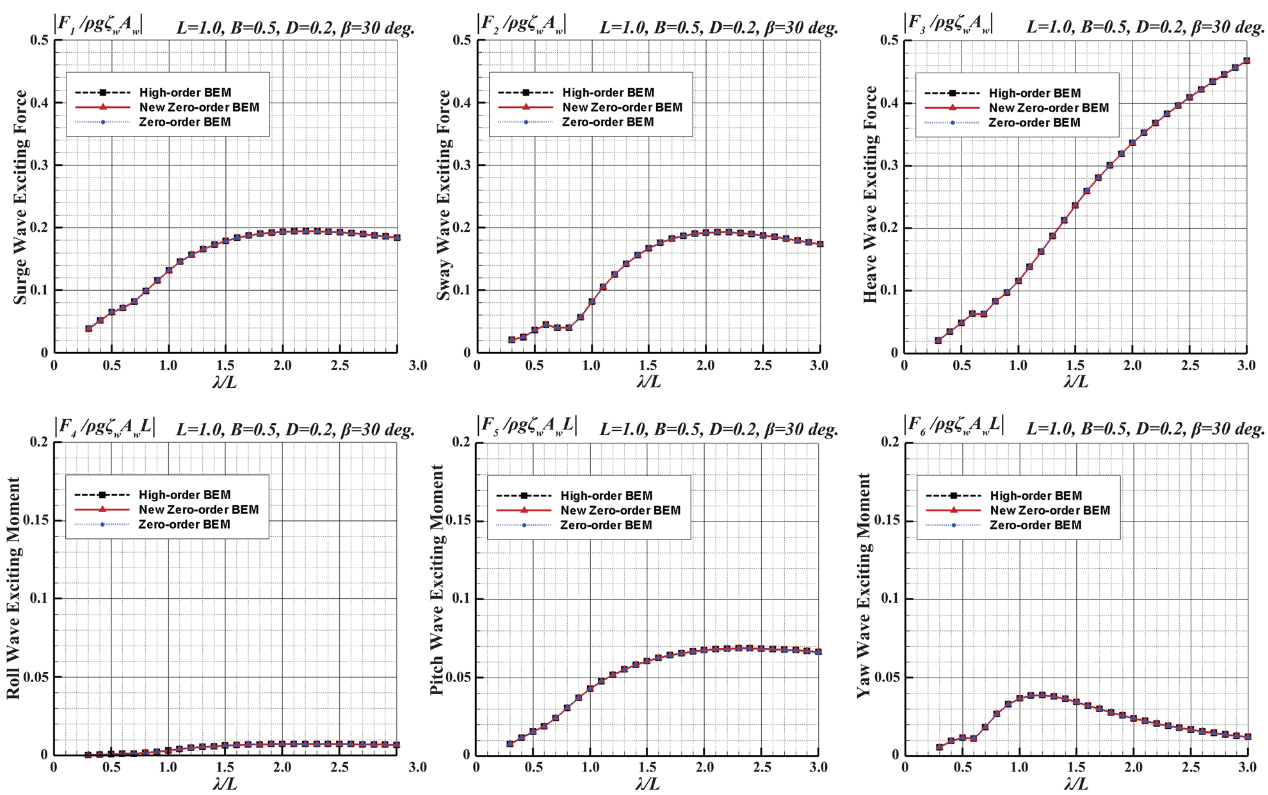

Fig. 7 Wave exciting forces and moments of single body ($\beta=30$ deg)

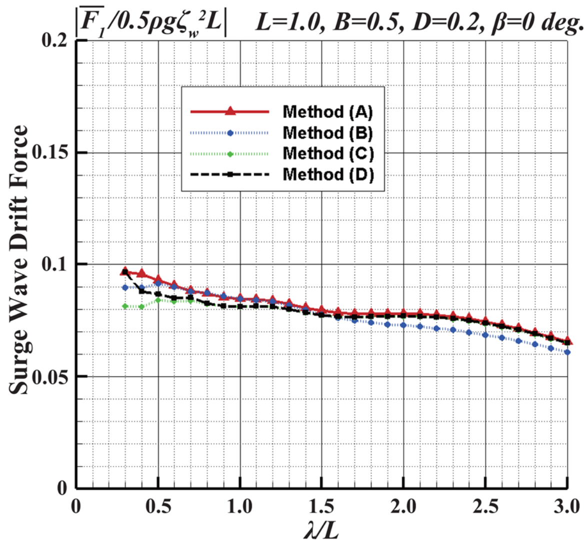

Fig. 8 Wave drift force of single body ($\beta = 0$ deg)

To compare, the results are compared to those which were obtained with the $N_E = 48 \times 48$ mesh. This convergence of varying λ/L values is tabulated in Table 1. For all λ/L, the results converged within 1% error for a mesh size greater than or equal to 30×30.

For the single floating body, fluid forces are gathered using the new constant panel method, HOBEM, and the conventional constant panel method, and compared afterward.

4.1.2 Wave Exciting Forces and Moments. The velocity potential is calculated using the three methods (new constant panel method, HOBEM, and conventional constant panel method). The wave exciting forces and moments (surge, $i=1$; sway, $i=2$; heave, $i=3$; roll, $i=4$; pitch, $i=5$; yaw, $i=6$) were calculated as follows:

$$F_i = -\iint_{S_H} p(x,y,z)n_i dS = \rho g \zeta_w \iint_{S_H} \phi_D(x,y,z)n_i dS \tag{44}$$

The nondimensional exciting forces and moments can be calculated as follows:

$$CF_i = \frac{F_i}{\rho g \zeta_w A_w} \quad (i = 1 \sim 3)$$
$$CF_i = \frac{F_i}{\rho g \zeta_w A_w L} \quad (i = 4 \sim 6) \tag{45}$$

Table 2 Percentage difference of the calculation accuracy by (A)-method–(C)-method ($\beta = 0$ deg surge)

λ/L	(A)	(B)	(C)
0.3	0.0%	6.9%	15.3%
0.7	−3.5%	−3.3%	1.6%
1.1	−3.6%	−3.3%	0.0%
1.5	−2.4%	−0.5%	0.0%
1.9	−1.6%	4.5%	0.0%
2.3	−1.1%	6.7%	0.2%
2.7	−0.9%	6.9%	0.3%

where ζ_w denotes the wave height, A_w denotes the water area.

The wave exciting forces and moments at both wave angles of incidence, $\beta = 0$ deg and 30 deg, are shown in Figs. 6 and 7, respectively. For all cases, the results obtained using the three methods are equal. Therefore, conventional constant panel method can be used to calculate wave exciting forces and moments, though the velocity potential on the water line cannot be accurately obtained. Furthermore, the new constant panel method also accurately calculates the wave exciting forces and moments.

4.1.3 Wave Drift Forces and Moment. The velocity potential is calculated using the three methods (new constant panel method, HOBEM and conventional constant panel method). Figure 8 shows the results of the surge drift force (angle of incidence $\beta = 0$ deg). Figure 9 shows the results of the surge drift force, sway drift force, and yaw drift moment (angle of incidence $\beta = 30$ deg).

The following four combinations of numerical methods are recorded for comparative analysis:

(A) New constant panel method + near-field method
(B) Conventional constant panel method + near-field method
(C) Conventional constant panel method + far-field method
(D) HOBEM + far-field method

Method (A) is the method this paper proposes. Method (B) is method (A) without utilization of the extrapolation function and without the isoparametric elements. Method (C) and method (D) are the conventional methods used to calculate wave drift forces.

Figures 8 and 9 show that the results obtained by the proposed method, method (A), agree well with method (C) and method (D), the conventional dependable simulation standards. Table 2 provides the percentage difference of the surge drift forces ($\beta = 0$ deg) obtained from the three methods compared to method (D); Table 3, the sway drift forces ($\beta = 30$ deg); and Table 4, the yaw drift moment ($\beta = 30$ deg).

Though method (B) sometimes produces acceptable results ($\beta = 0$ deg surge drift force), it consistently produces results with an error rate above 20%, even exceeding 60% ($\beta = 30$ deg yaw drift moment). Method (A) often returns results with an error rate

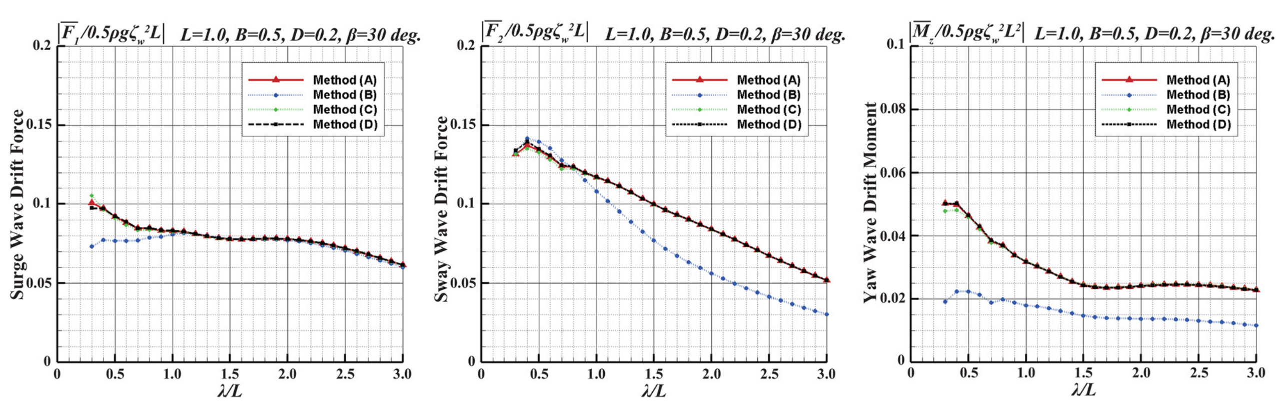

Fig. 9 Wave drift forces and moment of single body ($\beta = 30$ deg)

Table 3 Percentage difference of the calculation accuracy by (A)-method–(C)-method ($\beta = 30$ deg sway)

λ/L	(A)	(B)	(C)
0.3	1.8%	0.0%	1.8%
0.7	0.2%	−2.8%	1.9%
1.1	0.1%	11.1%	0.3%
1.5	0.0%	22.8%	0.1%
1.9	0.0%	31.7%	0.1%
2.3	0.0%	36.8%	0.2%
2.7	0.1%	39.8%	0.2%

Table 4 Percentage difference of the calculation accuracy by (A)-method–(C)-method ($\beta = 30$ deg yaw)

λ/L	(A)	(B)	(C)
0.3	−0.3%	61.8%	4.3%
0.7	0.6%	51.0%	1.6%
1.1	−0.1%	42.0%	−0.3%
1.5	−0.3%	39.5%	−0.9%
1.9	−0.3%	42.2%	−1.0%
2.3	−0.3%	45.0%	−0.9%
2.7	−0.3%	47.3%	−0.8%

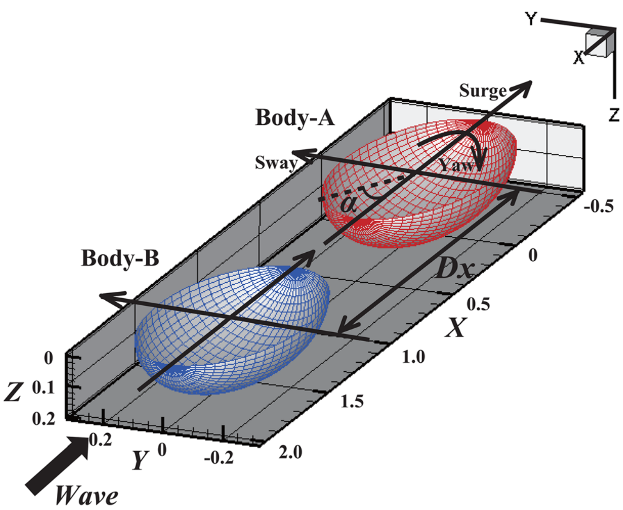

Fig. 10 Calculation model of two ellipsoid bodies in tandem

of less than 1%. Thus, this new numerical technique solves the two aforementioned issues regarding the use of the conventional constant panel method, allowing for the use of the near-field method to accurately calculate wave drift forces and moment.

4.2 Calculation of Two Floating Bodies. The same ellipsoid geometry is used for calculating hydrodynamic forces and moments for two floating bodies. As shown in Fig. 10, the ellipsoids are arranged in tandem along the Y-axis, where body-B makes first contact with the wave followed by body-A. D_X denotes the distance between the cores of the ellipsoids. The fluid forces of both floating bodies will be recorded and analyzed at as D_X varies from zero (single floating body) to 50 times the ellipsoid major diameter.

4.2.1 Wave Exciting Forces and Moments. Figure 11 shows the surge wave exciting force (left), heave wave exciting force (center), and pitch wave exciting moment (right) for body-A; Fig. 12 shows the same for body-B. The sway wave exciting force, roll wave exciting moment, and yaw wave exciting moment are omitted since the results were 0.

As shown in Fig. 11, all wave exciting forces and moment in body-A for two floating bodies were found to be lower than those of the single floating body. As the distance between the floating bodies increases, the wave exciting forces and moment approach the single body result. The reason for this phenomenon is the shield effect, which suggests a reduction in hydrodynamic interaction as the distance between the floating bodies increases. Figure 12 shows that the wave exciting forces and moment experienced by body-B vary from being larger and smaller than the single body results. This phenomenon is caused by the reflected wave effect of body-A.

4.2.2 Wave Drift Forces and Moment. Figures 13 and 14 show the surge wave drift forces for body-A and body-B for varying D_X values. The sway drift force and yaw wave drift moment are omitted since the results were 0.

Figure 13 shows a decrease of more than 50% in surge wave drift forces in body-A when $D_X = 2.0$ compared to the single body results. As the distance between the floating bodies increases, the hydrodynamic interaction decreases and approaches that of the single body result. Figure 14 shows that surge wave drift force of body-B remains unchanged for shorter wavelengths ($\lambda/L = 0.3$–1.0). For longer wavelengths ($\lambda/L = 2.0$–3.0), the same phenomenon occurs—as the distance increases, the surge drift force approximates that of the single body results.

5 Conclusion

This paper proposes a numerical technique, the new constant panel method, to address two issues in the usage of the conventional constant panel method. The first issue is the evaluation of

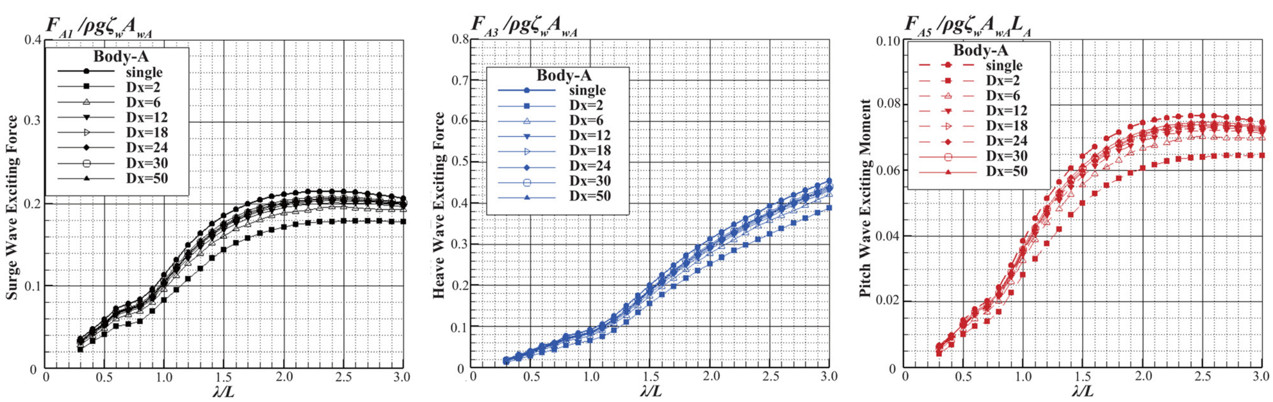

Fig. 11 Wave exciting forces and moments of body = A in different D_X

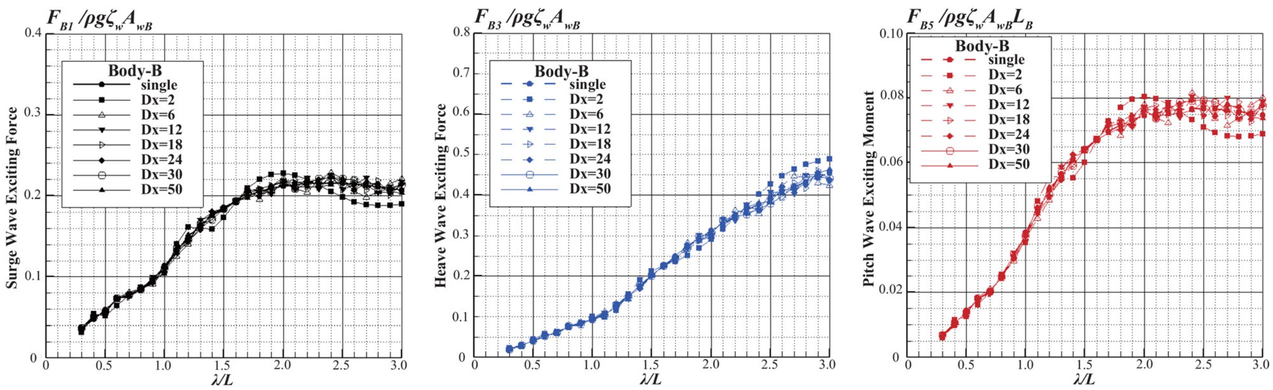

Fig. 12 Wave exciting forces and moments of body = B in different D_X

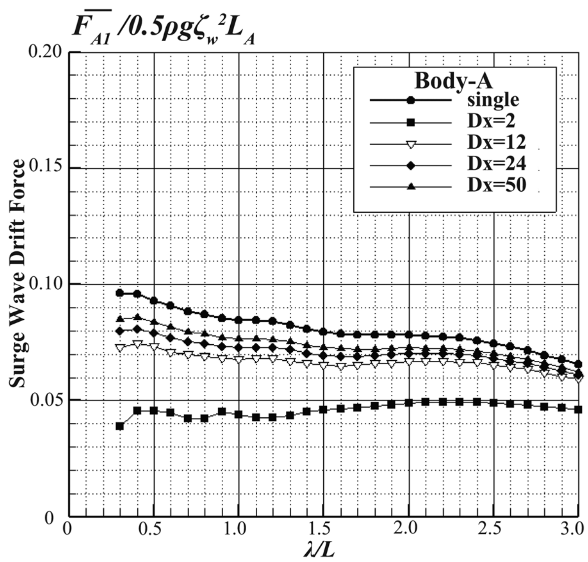

Fig. 13 Surge wave drift forces of body-A in different D_X

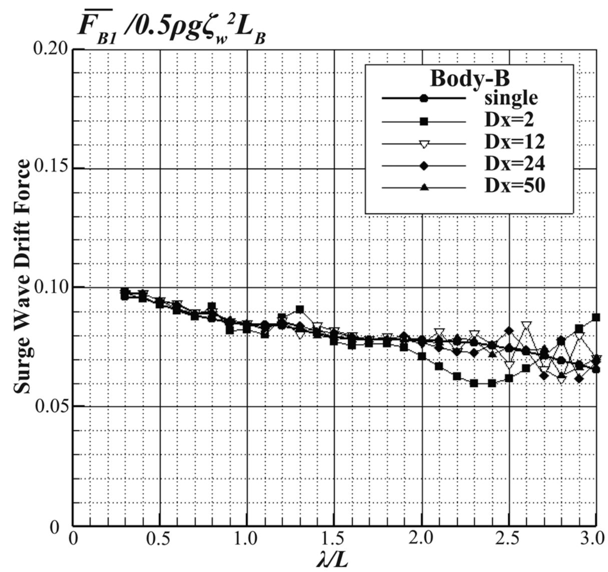

Fig. 14 Surge wave drift forces of body-B in different D_X

the velocity potential along the water line, and the other is evaluating velocity potential differentials with high precision. The new technique allows for usage of the near-field method to calculate the wave drift forces and moment. Floating bodies of ellipsoid geometry were used as examples to test and compare results of the new method. Fluid forces obtained from the new method, HOBEM, and the conventional constant panel method were compared. The new constant panel method was applied to calculate motions of the two floating bodies. Hydrodynamic interactions for the two floating bodies arranged in tandem different lengths were analyzed.

The following results were obtained for the single floating body simulation:

- The conventional constant panel method can be used to calculate wave exciting forces and moments (first-order forces), even though the velocity potential was not representative of the water line. Furthermore, wave exciting forces and moments can be obtained using the new constant panel method.
- In comparing drift wave forces and moment to the dependable standard HOBEM in combination with the far-field method, the conventional constant panel method in combination with the near-field method produces large discrepancies upward of a 60% difference, while the new constant panel method in combination with the near-field method consistently produces discrepancies of less than 1%.

The following results were obtained for the two floating bodies' simulation:

- The wave exciting forces and moment experienced by body-A (down-wave body) approximate the results of the single body when the distances between the bodies increase.
- When the distance between the floating bodies is twice the ellipsoid major diameter, surge wave drift forces in body-A (down-wave body) decreases by 50% compared to the results of the single body. As the distance between the floating bodies increases, the hydrodynamic interactions decrease and the wave drift forces approach results of the single body.

Acknowledgment

The authors would like to thank Y. Ikeda and T. Tsubogo for useful discussions on topics regarding this paper. My sincere gratitude to M. Kashiwagi for providing the numerical simulations of HOBEM. A part of this work has been published in the JSNAOE in Japanese [14].

References

[1] Newman, J. N., 1967, "The Drift Force and Moment on Ships in Waves," J. Ship Res., **11**(1), pp. 51–60.
[2] Maruo, H., 1960, "The Drift of a Body Floating on Waves," J. Ship Res., **4**, pp. 1–10.

[3] Kashiwagi, M., Kazuaki, E., and Hiroshi, Y., 2005, "Wave Drift Forces and Moments on Two Ships Arranged Side by Side in Waves," Ocean Eng., **32**(5–6), pp. 529–555.
[4] Pinkster, J. A., and van Oortmerssen, G., 1977, "Computation of the First and Second Order Wave Forces on Oscillating Bodies in Regular Waves," Second International Conference on Numerical Ship Hydrodynamics, Berkeley, CA, Sept. 19–21, pp. 136–156.
[5] Pinkster, J. A., 1979, "Mean and Low Frequency Wave Drifting Forces on Floating Structures," Ocean Eng., **6**(6), pp. 593–615.
[6] Pinkster, J. A., 1980, "Low Frequency Second Order Wave Exciting Forces on Floating Structures," Ph.D. thesis, TU Delft, Delft, The Netherlands.
[7] Takagi, M., and Arai, S., 1996, *Sea Kindliness Theory of Ship and Offshore Structure*, Seizando-Shoten Publishing, Tokyo, Japan (in Japanese).
[8] Kashiwagi, M., Takagi, K., Yoshida, H., Murai, M., and Higo, Y., 2003, *Practice-Fluid Mechanics*, Seizando-Shoten Publishing, Tokyo, Japan (in Japanese).
[9] Söding, H., 1993, "A Method for Accurate Force Calculations in Potential Flow," Ship Technol. Res., **40**(3), pp. 176–186.
[10] Söding, H., Shigunov, V., Schellin, T. E., and Moctar, O., 2014, "A Rankine Panel Method for Added Resistance of Ships in Waves," ASME J. Offshore Mech. Arct. Eng., **136**(3), p. 031601.
[11] Yan, H., and Liu, Y., 2011, "An Efficient High-Order Boundary Element Method for Nonlinear Wave–Wave and Wave-Body Interactions," J. Comput. Phys., **230**(2), pp. 402–424.
[12] Newman, J. N., 1986, "Distributions of Sources and Normal Dipoles Over a Quadrilateral Panel," J. Eng. Math., **20**(2), pp. 113–126.
[13] Kashiwagi, M., 2002, "Wave-Induced Local Steady Forces on a Column-Supported Very Large Floating Structure," Int. J. Offshore Polar Eng., **12**(2), pp. 98–104.
[14] Li, Q., Ikeda, Y., and Nihei, Y., 2016, "A Study on the Wave Drift Forces Calculation Based on BEM," J. Jpn. Soc. Nav. Archit. Ocean Eng., **23**, pp. 77–85 (in Japanese).